# Neurotoxic *unc-8* mutants encode constitutively active DEG/ENaC channels that are blocked by divalent cations

Ying Wang,[1] Cristina Matthewman,[1] Lu Han,[1] Tyne Miller,[2,3] David M. Miller III,[2,3] and Laura Bianchi[1]

[1]Department of Physiology and Biophysics, University of Miami, Miller School of Medicine, Miami, FL, 33136
[2]Department of Cell and Developmental Biology and [3]Neuroscience Program, Vanderbilt University, Nashville, TN 37232

Ion channels of the DEG/ENaC family can induce neurodegeneration under conditions in which they become hyperactivated. The *Caenorhabditis elegans* DEG/ENaC channel MEC-4(d) encodes a mutant channel with a substitution in the pore domain that causes swelling and death of the six touch neurons in which it is expressed. Dominant mutations in the *C. elegans* DEG/ENaC channel subunit UNC-8 result in uncoordinated movement. Here we show that this *unc-8* movement defect is correlated with the selective death of cholinergic motor neurons in the ventral nerve cord. Experiments in *Xenopus laevis* ooctyes confirm that these mutant proteins, UNC-8(G387E) and UNC-8(A586T), encode hyperactivated channels that are strongly inhibited by extracellular calcium and magnesium. Reduction of extracellular divalent cations exacerbates UNC-8(G387E) toxicity in oocytes. We suggest that inhibition by extracellular divalent cations limits UNC-8 toxicity and may contribute to the selective death of neurons that express UNC-8 in vivo.

The Journal of General Physiology

## INTRODUCTION

DEG/ENaC channel subunits (named after the degenerin MEC-4 and the mammalian epithelial $Na^+$ channel; Driscoll and Chalfie, 1991; Canessa et al., 1993) contain two transmembrane domains, a large extracellular loop and short intracellular N and C termini that form trimeric voltage-independent $Na^+$ or/and $Ca^{2+}$ channels. Crystal structure analysis of chicken ASIC1a revealed that three DEG/ENaC subunits come together to form a channel, and that the large extracellular domain of each subunit forms a "clenched-hand" structure that protrudes from the plasma membrane (Jasti et al., 2007). Structural and functional analysis has shown that this extracellular domain specifies channel regulation by protons and other ions, and that it undergoes substantial movement during channel gating (Jasti et al., 2007; Zhang et al., 2008; Li et al., 2009; Passero et al., 2009; Sherwood et al., 2009; Wang and Bianchi, 2009; Shi et al., 2011). DEG/ENaC channels are comprised of either homomeric or heteromeric trimers, and at least some DEG/ENaC channels are associated with auxiliary subunits (Lingueglia et al., 1997; Bianchi and Driscoll, 2002; Chelur et al., 2002; Goodman et al., 2002; Askwith et al., 2004).

DEG/ENaC channels are expressed in a wide variety of cell types including epithelial cells (Canessa et al., 1993), neurons (Bianchi and Driscoll, 2002), and glia (Wang et al., 2008; Hitomi et al., 2009; Calavia et al., 2010; Han et al., 2013), where they function to mediate physiological processes as diverse as $Na^+$ reabsorption (Hummler et al., 1996), memory formation, and sensory perception (Tavernarakis et al., 1997; Price et al., 2000, 2001; Sluka et al., 2003; Wemmie et al., 2003; Wang et al., 2008; Chandrashekar et al., 2010). Some DEG/ENaC channels, including *Caenorhabditis elegans* MEC-4 and mammalian ASIC1a, have been shown to undergo "hyperactivation" as a result of genetic mutations (Driscoll and Chalfie, 1991; García-Añoveros et al., 1995) and chronic exposure to protons (Xiong et al., 2004), respectively. In these conditions, DEG/ENaC channels switch to a high open probability mode that results in large whole cell currents (Goodman et al., 2002; Brown et al., 2007). The resultant influx of cations induces cell swelling and death through a mechanism that involves release of calcium from the ER and activation of calcium-sensitive proteases such as calpains and cathepsins (Xu et al., 2001; Syntichaki et al., 2002). Interestingly, both *C. elegans* MEC-4 and mouse ASIC1a show some calcium permeability, suggesting that, at least in some cases, calcium influx through hyperactivated DEG/ENaCs triggers the cell death program (Zhang and Canessa, 2002; Bianchi et al., 2004; Xiong et al., 2004).

Mutations in the *C. elegans* DEG/ENaC subunit UNC-8 have been isolated in genetic screens as uncoordinated animals (Brenner, 1974; Park and Horvitz, 1986; Shreffler

Y. Wang and C. Matthewman contributed equally to this paper.
Correspondence to Laura Bianchi: lbianchi@med.miami.edu



The Rockefeller University Press $30.00
J. Gen. Physiol. Vol. 142 No. 2 157–169
www.jgp.org/cgi/doi/10.1085/jgp.201310974

et al., 1995). The dominant mutants, *unc-8(n491)* and *unc-8(e15)*, of which both encode the single mutation UNC-8(G387E), display a strong backward movement defect. Microscopic analysis of *unc-8(n491)* and *unc-8(e15)* animals detected neuronal swelling during early larval development (Shreffler et al., 1995). Similar cell swelling resulting from hyperactivated DEG/ENaC channels such as MEC-4(d) (Driscoll and Chalfie, 1991) suggests that *unc-8(n491)* and *unc-8(e15)* may encode constitutively active UNC-8 channels. Cell swelling in these *unc-8(d)* mutants is less severe, however, than that observed for *mec-4(d)* animals. In addition, a majority of the affected motor neurons in *unc-8(d)* mutants appear to recover by the adult stage, whereas neurons that express MEC-4(d) channels typically undergo necrotic cell death (Driscoll and Chalfie, 1991; Shreffler et al., 1995). A milder neurotoxic phenotype is also caused by expression of MEC-10(d) in touch neurons (Huang and Chalfie, 1994). MEC-10 cannot form channels on its own but associates with MEC-4 to modulate its properties (Goodman et al., 2002). Thus, the milder neurotoxic phenotype of MEC-10(d) was interpreted to be the result of the MEC-10 accessory role in the channel complex.

We undertook this study to better define the neuronal toxicity of *unc-8(n491)*, *unc-8(e15)*, and *unc-8(n49)* (encoding A586T mutation) mutants and to establish the physiological properties of UNC-8(d) channels that they encode. We show that DA and DB motor neurons swell in *unc-8(n491)* L1 larval stage and that ∼35% of them degenerate by adulthood. We also show by expression in *Xenopus laevis* oocytes that UNC-8 forms homomeric channels and that neurotoxic UNC-8 mutations induce channel hyperactivation. However, we found that the overall current amplitude is small because of the high affinity blockage of UNC-8 channels by extracellular divalent cations. Removal of divalent cations results in strong currents and induces *Xenopus* oocyte cell death. Expression of an UNC-8 intragenic mutation that suppresses neuronal swelling reduces current amplitude. UNC-8(A586T), which corresponds to the relatively weak *unc-8(n49)* allele, is inhibited by extracellular calcium and acidic pH with higher affinity than the more toxic UNC-8(G387E). Collectively, our data are consistent with the proposal that hyperactive cation transport accounts for the neurotoxicity of UNC-8 gain-of-function mutants, and that this activity is likely regulated in vivo by extracellular divalent cations and pH.

## MATERIALS AND METHODS

### *C. elegans* culture

Nematode strains were maintained at 20°C on standard nematode growth medium seeded with *Escherichia coli* strain OP50 (Brenner, 1974). Wild-type animals were N2 Bristol. Strains used in this work include: *CZ1200 (juIs76 [unc-25p::*GFP + *lin-15(+)] II;lin-15B(n765) X*) to label GABA motor neurons with GFP and RP1(*trIs10 [myo-3p::MB::YFP + myo-2p::YFP + ceh-23::HcRed + unc-25::*dsRed + *unc-129nsp::*CFP*]* I) to label GABA motor neurons with dsRed and cholinergic DA/DB neurons with CFP. *unc-8(n491)* IV was crossed into the marker strains to generate *NC2782 [punc-25::*GFP *(II); unc-8(n491) IV]* and *NC2799 [unc-8(n491) IV; trIs10 [myo-3p::MB::YFP + myo-2p::YFP + ceh-23::HcRed + unc-25:: DsRed + unc-129nsp::*CFP*] I*].

### Microscopy

Animals were immobilized with 15 mM levamisole on 2% agarose pads with M9 buffer as described previously (Smith et al., 2012). L1 animals were imaged with a microscope (Axioplan; Carl Zeiss) equipped with a camera (ORCA; Hammamatsu) and ImageJ Micro-Manager software. DIC images of ventral cord motor neurons were collected with a 100× oil objective; young adult animals were evaluated with a 63× oil objective. Images in Fig. 1 (C and D) were acquired with a confocal microscope (TCS SP5; Leica). Z stacks were collected with a 40× oil objective (1 µm/step). Single-plane projections were generated with Application Suite Advanced Fluorescence software (Leica). Insets of the CFP-labeled DA/DB neurons shown in Fig. 1 (C and D) were generated with the ImageJ plug-in "straighten curved objects" (Kocsis et al., 1991). Image overlays were performed with Adobe Photoshop.

### Cell-swelling analysis

To evaluate ventral cord motor neurons in the L1 stage for potential swelling, *punc-25::*GFP was used to mark GABA neurons in wild-type and *unc-8(n491)* animals. To generate synchronized populations of L1 larvae, 100 wild-type (*CZ1200*) and *NC2782 [punc-25::*GFP;*unc-8(n491)]* adults were picked to single 60-mm plates and allowed to lay eggs for 1 h. The midpoint of the hour was considered to be t = 0. Plates were maintained at 20°C. At 18 h after lay, early L1 animals were picked from plates and imaged (as above) on a microscope (Axioplan; Carl Zeiss).

### Scoring embryonic motor neurons in the adult ventral nerve cord

*RP1 (trIs10)* was used to visualize embryonic motor neurons (DA, DB, DD) in the ventral nerve cord in wild-type and *unc-8(n491)* adults. CFP-labeled DA/DB neurons and dsRed-labeled DD neurons were scored in the ventral cord regions between DD1 through DD6. Results were pooled from three separate experiments.

### Molecular biology

UNC-8 cDNA was cloned by RT-PCR using the one-step RT-PCR kit Titanium (Takara Bio Inc.) in two parts. We cloned the last ∼1,500 bp (from the HincII site to the stop codon) using UNC-8–specific primers designed according to the UNC-8–predicted cDNA sequence available on WormBase, and the 5′ end (up to the HincII site) using a reverse-specific primer and the splice leader primer SL1 (Graham et al., 1988) (Fig. S2). Total RNA from a *C. elegans* mixed-age population was used as template. PCR products were initially cloned into TOPO PCR2.1 vector for sequence verification and amplification. Sequence-verified cDNA fragments were then ligated together into PGEM vector (Goodman et al., 2002) to reconstitute the full-length UNC-8 cDNA. Mutations were introduced in UNC-8 cDNA sequence using the Quickchange mutagenesis kit (Agilent Technologies) according to the manufacturer's procedures. Mutant DNA were then sequenced and used for in vitro cRNA synthesis.

### Oocyte expression and electrophysiology

cRNAs were synthesized using T7 mMESSAGE mMACHINE kit (Invitrogen). cRNAs were then purified and run on denaturating agarose gels for size and integrity verification. cRNA quantification was performed spectroscopically. Stage V–VI oocytes were selected among multi-staged oocytes dissected by a 2-h collagenase

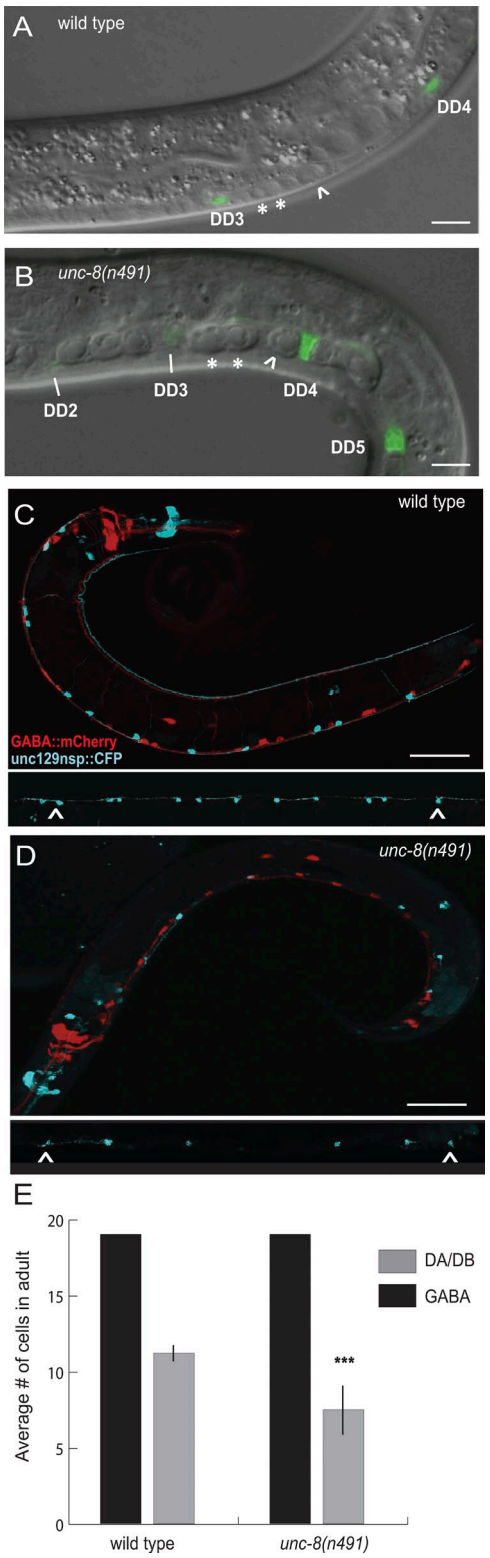


**Figure 1.** Selective degeneration of ventral cord cholinergic motor neurons in *unc-8(n491)* animals. DIC images of L1 larval ventral nerve cords of (A) wild-type versus (B) *unc-8(n491)* animals. Cholinergic DA and DB motor neurons (asterisks) and P cell precursor (arrowhead) appear swollen in *unc-8(n491)* versus wild type. DD GABA motor neurons are labeled with *punc-25::*GFP. Bar, 1 µm. (C and D) DD/VD GABAergic motor neurons are marked with *punc-25::*dsRed (red) and DA/DB neurons are labeled with *unc-129nsp::*CFP (blue) in (C) wild-type and (D) *unc-8(n491)* young adult animals. Insets show linearized view of DA/DB motor neurons. Bars, 25 µm. (E) GABAergic and DA/DB motor neurons were counted in the ventral cord region between DD1 and DD6 (arrowheads in C and D; see also Fig. S1). *unc-8(n491)* animals ($n$ = 14) contain the full complement of 19 DD/VD GABAergic motor neurons but are missing a significant fraction (~36%) of the 11 DA/DB motor neurons from this region of the adult ventral nerve cord (wild type; $n$ = 24). ***, P = 3 × E-11 by $t$ test.

treatment (2 mg/ml in $Ca^{2+}$-free OR2 solution) from *Xenopus* ovaries (provided by G. Dahl or C.W. Luetje, University of Miami, Coral Gables, FL). Oocytes were injected with 10 ng/oocyte of each cRNA and incubated in OR2 medium plus 300 µM amiloride. OR2 solution consists of 82.5 mM NaCl, 2.5 mM KCl, 1 mM $CaCl_2$, 1 mM $MgCl_2$, 1 mM $Na_2HPO_4$, 0.5 g/liter polyvinyl pyrolidone, and 5 mM HEPES, pH 7.2, supplemented with penicillin and streptomycin (0.1 mg/ml) and 2 mM Na-pyruvate at 20°C for 2–3 d before recordings. Currents were measured using a two-electrode voltage-clamp amplifier (GeneClamp 500B; Axon Instruments) at room temperature. Electrodes (0.2–0.5 MΩ) were filled with 3 M KCl, and oocytes were perfused with a physiological NaCl solution containing (mM) 100 NaCl, 2 KCl, 1 $CaCl_2$, 2 $MgCl_2$, and 10 HEPES, pH 7.2. The divalent cation–free plus EGTA NaCl solution contained (mM): 110 NaCl, 2 KCl, 1 EGTA, and 10 HEPES, pH 7.2. $CaCl_2$ was added to this solution to reach the desired concentrations (Schoenmakers et al., 1992). pH was adjusted at the indicated values using NMDG-Cl or HCl. When we tested solutions at pH lower than 6, we used 10 mM Mes instead of 10 mM HEPES to buffer the solutions. The divalent cation–free NaCl solution contained (mM): 110 NaCl, 2 KCl, and 10 HEPES, pH 7.2. $MgCl_2$ was added to this solution to reach the desired concentrations. The solution to test calcium permeability contained (mM): 73 $CaCl_2$, 2 KCl, and 10 HEPES, pH 7.2. The solutions to test UNC-8(G387E) selectivity contained (mM): 112 NaCl (LiCl, KCl, or NMDG-Cl), 1 EGTA, and 10 HEPES, pH 7.2. The oocyte membrane was clamped at −30 mV and stepped from −160 to +100 mV. Amiloride was added to the solutions from a stock of 10 mM, except for when 1 and 5 mM amiloride were used. In this case, amiloride was dissolved directly into the perfusing solution. Saturating concentration of amiloride (1 and 5 mM for experiments in physiological and divalent-free solutions, respectively) was added at the end of each experiment to make sure that endogenous/leak currents were similar in amplitude to noninjected oocytes within each oocyte batch. Oocytes that had larger endogenous/leak currents were not further analyzed. We used the pCLAMP suite of programs (Axon Instruments) for data acquisition and analysis. Currents were filtered at 200 Hz and sampled at 1 kHz.

### Scoring of cell death in *Xenopus* oocytes

Occytes were incubated in regular OR2 or OR2 containing 5 µM $Ca^{2+}$ plus or minus 500 µM amiloride for 24 h in individual wells (96-well plate), after injection with UNC-8 wild-type and UNC-8 (G387E) cRNAs and overnight incubation in regular OR2. After a 24-h incubation, oocytes were examined under the dissection microscope to establish if they were still intact. Oocytes were scored as "intact" if no cytoplasmic material was visible outside the oocyte.

### Online supplemental material

Fig. S1 shows the fraction of *unc-8(n491)* animals that lack a given DA, DB, or DD motor neuron versus the location of each motor neuron along the ventral nerve cord from anterior (DD1) to posterior (DD6). Fig. S2 shows UNC-8 protein sequence and alignment with other DEG/ENaC channels, *unc-8* gene structure,

sequence of the first two exons, and corresponding translation and location of the mutations studied. The online supplemental material is available at http://www.jgp.org/cgi/content/full/jgp.201310974/DC1.

## RESULTS

### Cholinergic motor neurons swell and a fraction of them die in *unc-8(n491)* mutants

We observed significant cell swelling in the ventral nerve cords of *unc-8(n491)* L1 stage larvae (Fig. 1). Swollen cells were visible in most *unc-8(n491)* animals at this stage but were rarely observed later in larval development. Swollen cells were also detected in other body regions (e.g., PVC neuron). Our results agree with a previous report that described transient swelling in the ventral nerve cord of L1 stage *unc-8(n491)* and *unc-8(e15)* animals (Shreffler et al., 1995). The ventral nerve cords of newly hatched L1 larvae contain three types of motor neurons: the cholinergic DAs (nine neurons), DBs (seven neurons), and GABAergic DDs (six neurons). We relied on the invariant locations of each member of these motor neuron classes (White et al., 1986) and the GABA-specific marker, *unc-25::*GFP, to determine that swelling is limited to DA and DB motor neurons and was never observed for the DD class in *unc-8(n491)* L1 animals (Fig. 1 B). We also noted occasional swelling of P cell precursors in the ventral nerve cord (Fig. 1 B). The motor neuron–specific effects are correlated with our finding that a fraction of DA and DB motor neurons (~36%) is missing from the adult ventral nerve cord, but no absences were observed for DD motor neurons (Fig. 1, C–E, and Fig. S1). The death of DA and DB motor neurons was not previously detected from counts of ventral cord cell nuclei stained with the DNA dye DAPI perhaps because this effect is limited to <10% of all ventral cord motor neurons in the adult and therefore difficult to detect with this approach (Shreffler et al., 1995). Our results suggest that constitutive UNC-8 activity can result in cell death and is thus consistent with similar observations for dominant mutants of the DEG/ENaC channels DEG-1 and MEC-4 (Chalfie and Wolinsky, 1990; Driscoll and Chalfie, 1991).

### UNC-8(G387E) encodes a hyperactivated mutant channel with strong outward rectification

Tavernarakis et al. (1997) showed that *unc-8* encodes a DEG/ENaC subunit and that both *n491* and *e15* alleles contain the G387E mutation. G387 is located in the UNC-8 extracellular domain in a poorly conserved loop of the "finger" domain (Gessmann et al., 2010) (Fig. S2, A and C). The neuronal swelling phenotype typical of neurons expressing hyperactive DEG/ENaC channels such as MEC-4(d) (Driscoll and Chalfie, 1991) suggested that the G387E mutation may result in a hyperactive UNC-8 channel. To test this hypothesis, we cloned UNC-8 cDNA for heterologous expression in *Xenopus* oocytes. Using the splice leader sequence primer SL1 (Graham

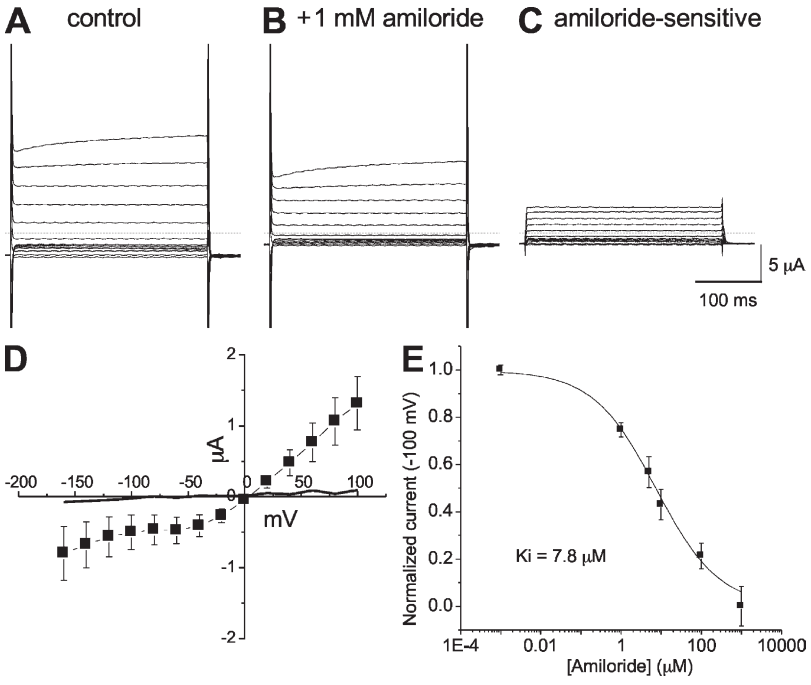


**Figure 2.** Amiloride-sensitive currents in UNC-8 (G387E)–expressing oocytes. (A) Example of ionic currents recorded in an oocyte expressing UNC-8(G387E) perfused with a NaCl physiological solution. Currents were elicited by voltage steps from −160 to +100 mV in 20-mV increments. The holding potential was −30 mV. (B) The same oocyte shown in A was perfused with NaCl physiological solution plus 1 mM amiloride. (C) Amiloride-sensitive currents. Currents obtained by subtracting the amiloride-resistant current from the total current are shown here. Dashed lines represent the zero current level. The outward amiloride-resistant current is likely oocytes endogenous current, which varies in amplitude from batch to batch of oocytes. (D) Current–voltage relationship of amiloride-sensitive currents in UNC-8(G387E)–expressing oocytes ($n$ = 5). Note the strong inward rectification at negative voltages. The solid line represents the amiloride-sensitive current recorded from an oocyte injected with wild-type UNC-8. (E) Amiloride dose–response curve. Currents recorded in amiloride at −100 mV were normalized against the currents recorded in NaCl physiological solution at −100 mV. Data points were fitted by Hill equation, which gave a Ki of 7.8 µM and an $n$ value of 0.5 ($n$ = 6). Data are expressed as mean ± SE.

et al., 1988), we identified an UNC-8 transcript that differed from the predicted gene structure (WormBase) in its first two exons (Fig. S2 B) as the most abundant UNC-8 mRNA. Using this UNC-8 cDNA as a template, we generated the UNC-8(G387E) mutant and expressed wild-type and mutant UNC-8 in *Xenopus* oocytes for electrophysiological analysis. We found that oocytes injected with wild-type UNC-8 did not produce currents above the background level. In contrast, UNC-8(G387E)–injected oocytes expressed an amiloride-sensitive current that reversed at ~0 mV (Fig. 2, A–D). These results are consistent with the idea that the G387E mutation enhances UNC-8 channel cation transport above the wild-type level and thus corresponds to a "hyperactive" mutation. From a dose–response curve, we calculated an amiloride Ki of 7.8 µM at −100 mV, as expected for a current that depends on DEG/ENaC channel activity (Fig. 2 E). Interestingly, UNC-8(G387E) currents displayed a strong outward rectification with larger values for positive potentials than for voltage clamps below 0 mV.

### UNC-8(G387E) currents are larger in divalent cation–free solution

The outward rectification of the amiloride-sensitive current in UNC-8(G387E)–expressing oocytes (Fig. 2 D) resembles that of other hyperactive DEG/ENaC channels including *C. elegans* UNC-105(d) and MEC-4(d) (García-Añoveros et al., 1998; Bianchi et al., 2004; Brown et al., 2008) that are negatively regulated by extracellular calcium. To test UNC-8(G387E) for similar regulation, we perfused oocytes with a solution prepared without divalent cations, and with a solution without divalent cations to which 1 mM EGTA was added to chelate residual calcium. In these divalent cation–free solutions, the UNC-8(G387E) current did not rectify and showed a linear response to voltage from −160 to +100 mV (Fig. 3, A–D). Strikingly, currents were also ~20 times larger both when the membrane was hyperpolarized and depolarized, suggesting that both inward and outward currents are blocked by divalent cations (Fig. 3 D). This behavior differs significantly from that of UNC-105(d) and MEC-4(d) channels for which

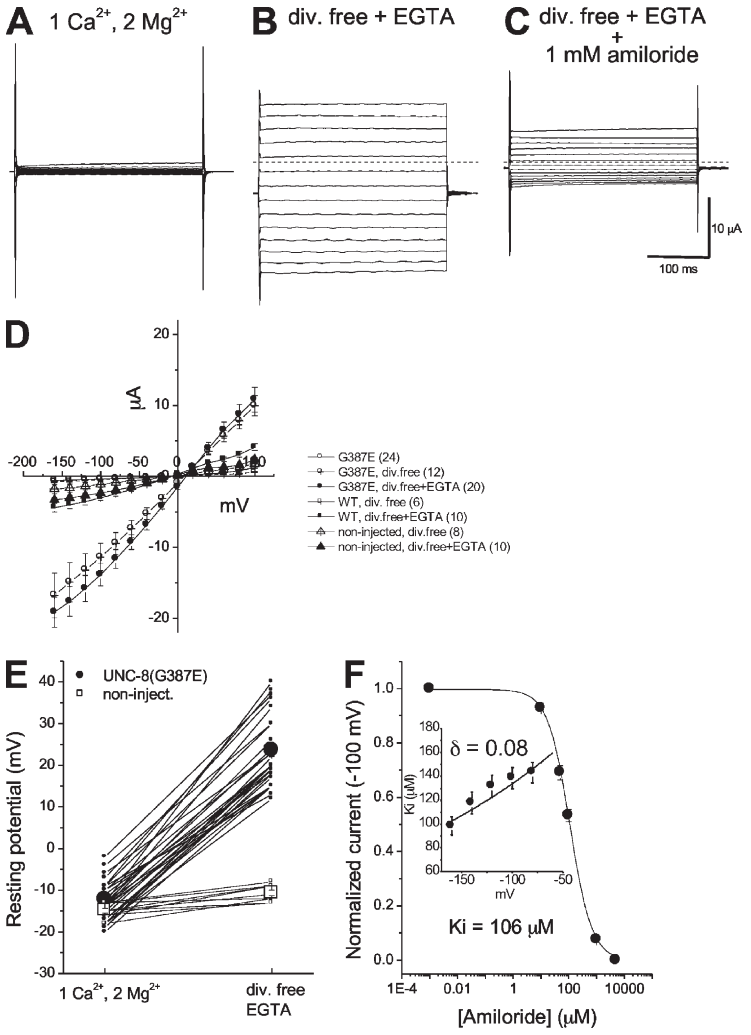


**Figure 3.** UNC-8(G387E) currents are larger in divalent cation–free solution. (A) Example of currents recorded in an oocyte injected with UNC-8(G387E) and perfused with NaCl physiological solution, which contains 1 mM $CaCl_2$ and 2 mM $MgCl_2$. Currents were stimulated by voltage steps from −160 to +100 mV in 20-mV increments. The holding potential was −30 mV. (B) The same oocyte shown in A was perfused with a divalent cation–free NaCl solution containing 1 mM EGTA. Currents were recorded with the same voltage protocol used in A. (C) Currents were recorded from the same oocyte in divalent cation–free EGTA solution plus 1 mM amiloride. Dashed lines represent the zero current level. (D) Current–voltage relationships from noninjected oocytes and oocytes injected with UNC-8 or UNC-8(G387E), and perfused with either the NaCl physiological solution or the divalent cation–free or divalent cation–free plus EGTA NaCl solution, as indicated. The number of oocytes tested is shown in parentheses. (E) Shift in the oocyte resting potential upon switching from NaCl physiological solution (1 mM $CaCl_2$ and 2 mM $MgCl_2$) to divalent cation–free plus EGTA NaCl solution for noninjected oocytes (open squares; $n = 9$) and oocytes injected with UNC-8(G387E) (closed circles; $n = 32$). Small symbols and lines correspond to measurement from individual oocytes, and large symbols are means ± SE. (F) Amiloride dose–response curve obtained from oocytes injected with UNC-8(G387E) and perfused with divalent cation–free plus EGTA NaCl solution. Data points were fitted by Hill equation, which gave a Ki of 106 µM and an $n$ value of 1. The inset shows the voltage dependence of amiloride blockade. Data points were fitted using the Woodhull model, which gave a δ of 0.08 (Woodhull, 1973). Data are expressed as mean ± SE ($n = 8$).

inhibition by extracellular calcium is limited to currents at negative membrane potentials. We conducted similar experiments in divalent cation–free solution for oocytes injected with wild-type UNC-8 but did not detect currents above the oocyte background level, even when twice as much cRNA was injected (Fig. 3 D and not depicted). These results suggest that wild-type UNC-8 requires a specific stimulus to be activated. Several members of the DEG/ENaC family are gated by extracellular protons (Bianchi and Driscoll, 2002). Thus, we tested whether wild-type UNC-8 was activated by perfusion with a solution at pH 5. However, we found no increase of currents above the background level, suggesting that UNC-8 is gated by stimuli other than protons (not depicted). One possibility is that UNC-8 is gated by mechanical forces, as suggested by Tavernarakis et al. (1997).

Because removal of extracellular divalent cations results in a large increase in UNC-8(G387E) current, we predicted that the resting potential of these oocytes would become more depolarized, consistent with $Na^+$ becoming the predominant cation transported into the oocyte, upon perfusion with the divalent cation–free plus EGTA solution. Indeed, we found that oocytes injected with UNC-8(G387E) underwent a significant depolarization with the switch from physiological to divalent cation–free plus EGTA NaCl solution. Conversely, noninjected oocytes depolarized only a few millivolts under the same experimental conditions (Fig. 3 E). Amiloride binding was substantially weakened in the divalent cation–free plus EGTA solution with a Ki of 106 µM (compare Fig. 3 F with Fig. 2 E). Interestingly, although amiloride binding appears to display negative cooperativity in physiological solution (fit with Hill's equation, $n = 0.5$; Fig. 2 E), it shows no cooperativity in the divalent cation–free plus EGTA solution ($n = 1$). Collectively, these results suggest that extracellular divalent cations influence amiloride binding and/or blockage.

### Reduction of extracellular divalent cations results in death of oocytes expressing UNC-8(G387E)

Although UNC-8(G387E) generates strongly outwardly rectifying currents, MEC-4(d) currents are not outwardly rectifying (Goodman et al., 2002). Moreover, although removal of divalent cations from the extracellular solution has little effect on MEC-4(d) currents, UNC-8(G387E) currents are increased >20-fold by this treatment (Fig. 3, A–D) (Bianchi et al., 2004; Brown et al., 2008). Interestingly, although MEC-4(d) causes death of all six touch neurons in which it is expressed, UNC-8(G387E) appears to kill only a fraction of DA/DB motor neurons (Fig. 1 E and Fig. S1). Thus, we hypothesized that the amplitude of the current may reflect the level of toxicity of these two mutant channels. We also predicted that relief or reduction of the divalent block of UNC-8(G387E) would exacerbate toxicity. To test this idea, we incubated *Xenopus*

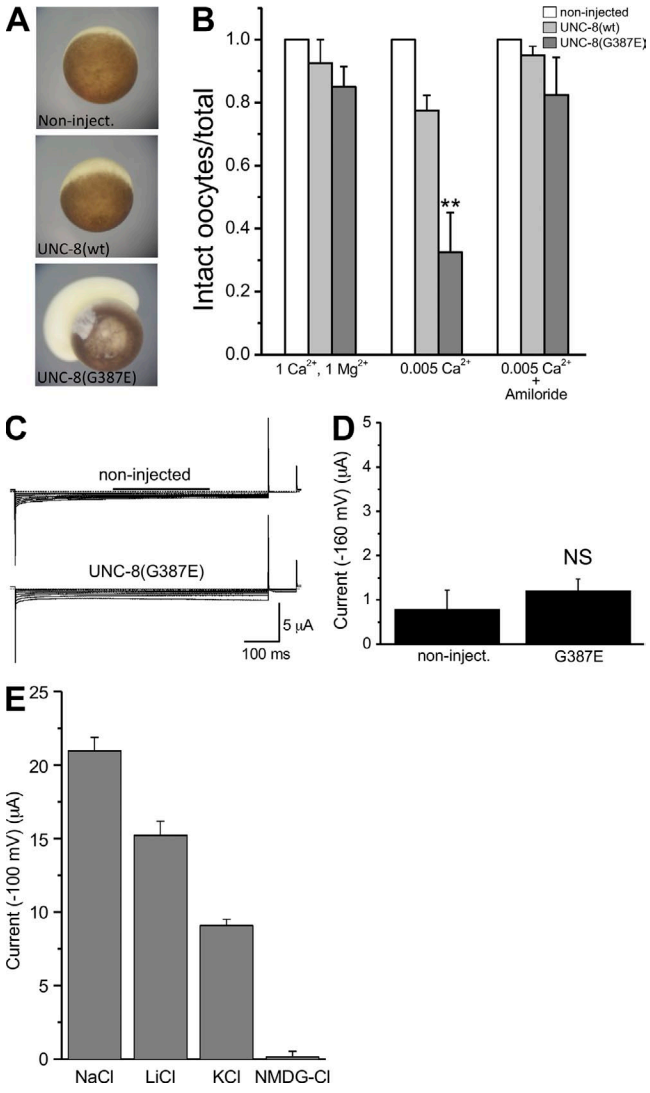


**Figure 4.** Cell death and UNC-8(d) permeability properties. (A) Representative photographs of a noninjected oocyte (top), oocyte-injected UNC-8 wild type, and an UNC-8(G387E) (middle and bottom panels, respectively) incubated for 24 h in OR2 solution containing 5 µM calcium and no magnesium. Note the lysis of the oocyte-expressing UNC-8(G387E). (B) Quantification of the ratio of oocytes that are intact after a 24-h treatment in OR2 containing 5 µM calcium. Values are averages of four independent injections with 10 oocytes in each replicate. Amiloride was added to a final concentration of 500 µM. Values are mean ± SE. **, $P \leq 0.01$ by ANOVA. (C) Example of currents recorded in a noninjected oocyte (top) and an oocyte injected with UNC-8(G387E) perfused with a solution whose only permeant cation was calcium. Voltage steps were from −160 to −40 mV from a holding potential of 0 mV. (D) Average current amplitudes at −160 recorded from noninjected oocytes and oocytes injected with UNC-8(G387E) perfused with the calcium solution. Note that the oocyte-endogenous $Ca^{2+}$-activated $Cl^-$ current is not activated in either sample (Bianchi et al., 2004). Data are expressed as mean ± SE ($n = 8$). NS, not statistically different. (E) Average current amplitude recorded at −100 mV in oocytes injected with UNC-8(G387E) perfused the solutions indicated on the x axis. Data are expressed as mean ± SE ($n = 12$, 12, 12, and 9, respectively).

oocytes expressing UNC-8(G387E) in OR2 solution containing only 5 μM $Ca^{2+}$ and no $Mg^{2+}$; 68% of these oocytes appeared swollen and burst after 24 h of incubation. In contrast, the same treatment did not cause bursting of noninjected oocytes or oocytes injected with wild-type UNC-8 (Fig. 4, A and B). The addition of 500 μM amiloride was protective and rescued oocytes from bursting (Fig. 4 B). These results suggest that the block exerted by divalent cations limits the toxicity of the UNC-8(G387E) mutant channel.

### UNC-8(G387E) permeability properties

Neurotoxic DEG/ENaC channels MEC-4(d) and ASIC1a show some permeability to $Ca^{2+}$ ions (Bianchi et al., 2004; Xiong et al., 2004). However, it is not clear whether $Ca^{2+}$ permeability is necessary for DEG/ENaC-induced neurotoxicity. We tested whether neurotoxic UNC-8 (G387E) is $Ca^{2+}$ permeable by perfusing oocytes with a $CaCl_2$ solution and by monitoring the activation of the endogenous $Ca^{2+}$-activated $Cl^-$ current (Bianchi et al., 2004). However, we did not detect currents above the background level (Fig. 4, C and D), indicating that UNC-8(G387E) is not permeable to $Ca^{2+}$ ions. We further analyzed UNC-8(G387E) selectivity properties by measuring current amplitude in oocytes perfused with extracellular solutions in which NaCl was replaced with LiCl, KCl, and NMDG-Cl. We found that the selectivity series for UNC-8(G387E) for monovalent cations was $Na^+ > Li^+ > K^+ >> NMDG^+$ (Fig. 4 E). The relatively high $K^+$ permeability may explain why the reversal potential of the UNC-8(G387E) was closer to 0 mV than expected for a selective $Na^+$ channel. To conclude, UNC-8(G387E) is permeable to both $Na^+$ and $K^+$, but it is not permeable to the larger monovalent cation $NMDG^+$ or to the divalent cation $Ca^{2+}$.

### Calcium and magnesium sensitivity of UNC-8(G387E)

For quantitative measurements of calcium and magnesium affinity, we measured UNC-8(G387E) currents while perfusing the oocytes with increasing concentrations of each divalent cation. These experiments showed that UNC-8(G387E) is blocked by extracellular calcium with a Ki of 6 μM at −100 mV (Fig. 5, A–C). To establish whether calcium binds the channel within the membrane electric field, we determined the voltage dependence of Ki. By fitting data points with the Woodhull model (Woodhull, 1973), we established that the calcium-binding site in UNC-8(G387E) is 6% within the membrane electric field (Fig. 5 D). Note that $Ca^{2+}$ blocks the outward current as well (Fig. 5 B). This result

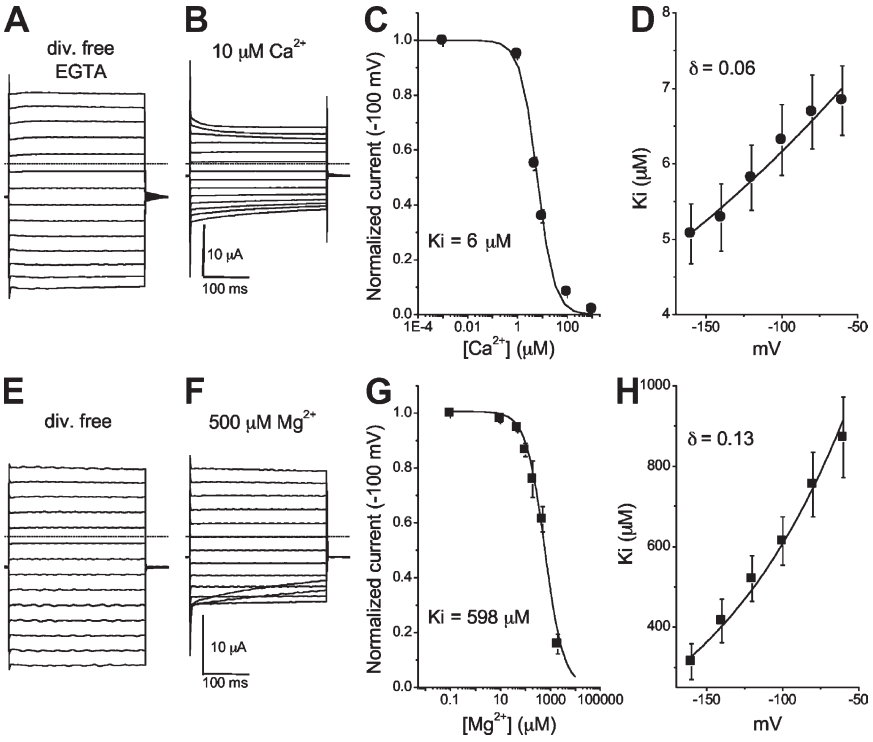


**Figure 5.** UNC-8(G387E) calcium and magnesium sensitivity. (A) Example of ionic currents recorded in an oocyte injected with UNC-8(G387E) and perfused with the divalent cation–free plus EGTA NaCl solution. The voltage protocol from Fig. 3 A was used here. (B) The same oocyte was perfused with the NaCl solution containing 10 μM $CaCl_2$. (C) Calcium dose–response curve. Currents were recorded at −100 mV in oocytes perfused with increasing concentrations of extracellular calcium. Currents in the presence of calcium were normalized for the current recorded in the same oocyte in divalent cation–free plus EGTA NaCl solution. Before normalization, all currents were leak subtracted. Data points were fitted with a sigmoidal curve for a Ki of 6 μM ($n$ = 8). (D) Voltage dependence of calcium block. The Ki for calcium was plotted against the voltage. Data points were fitted using the Woodhull model; the δ value was 0.06 ($n$ = 7). (E) Same as in A, except that the divalent-free solution did not contain EGTA. (F) The same oocyte shown in E was perfused with the NaCl solution containing 500 μM $MgCl_2$. (G) Magnesium dose–response curve. Data points were derived as in C. Fitting with a sigmoidal curve gave a Ki value of 598 μM ($n$ = 11). (H) The Ki for magnesium block was plotted against the voltage. Data points were fitted by the Woodhull model; the δ value was 0.13 ($n$ = 9).

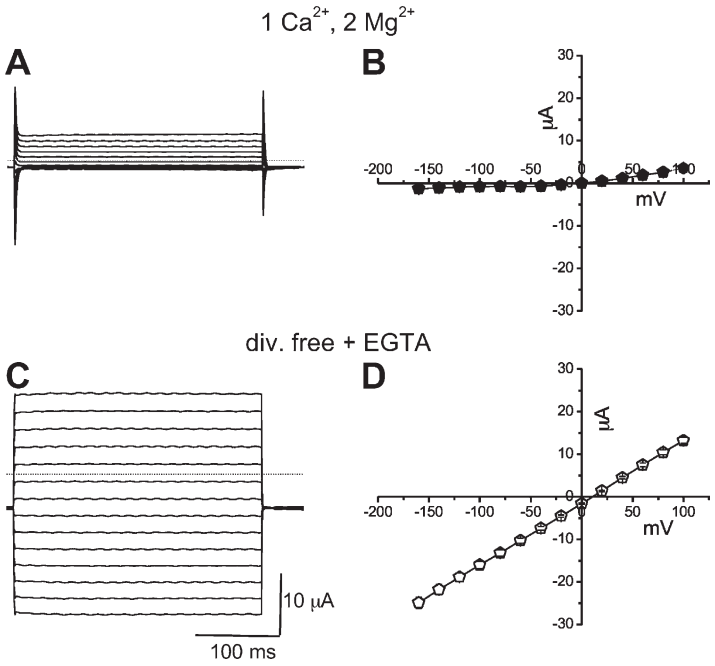


**Figure 6.** Calcium and magnesium block UNC-8(A586T) currents. (A) Example of currents stimulated by voltage steps from −160 to +100 mV in an oocyte injected with UNC-8(A586T); the holding potential was −30 mV. The oocyte was perfused with a physiological NaCl solution containing 1 mM $CaCl_2$ and 2 mM $MgCl_2$. (B) Average current–voltage relationships obtained from currents similar to the ones shown in A ($n = 6$). (C) The same oocyte shown in A was perfused with the divalent cation–free plus EGTA NaCl solution. (D) Average current–voltage relationship obtained from currents similar to the ones shown in C ($n = 6$).

suggests either that $Ca^{2+}$ binds within a crevice of the channel from where it cannot escape during membrane depolarization, or that the channel changes conformation once $Ca^{2+}$ is bound, thereby trapping the ion. On the basis of these results, we conclude that $Ca^{2+}$ block of the outward current likely accounts for the inhibition of outward current in physiological solution.

UNC-8(G387E) was blocked by magnesium with a Ki of 598 μM at −100 mV (Fig. 5, E–G). Interestingly, the voltage dependence of magnesium blockage is suggestive of a binding site deeper within the membrane electric field as compared with calcium. Indeed, by fitting data points with the Woodhull model, we obtained a δ of 0.13 (δ was 0.06 for calcium) (Fig. 5 H). Interestingly, $Mg^{2+}$ does not block the outward current (Fig. 5 F), suggesting that $Mg^{2+}$ is dislocated from its binding site upon depolarization. Collectively, our data show that UNC-8(G387E) is blocked by extracellular calcium and magnesium. However, the channel is more sensitive to calcium, and the two ions appear to bind to different sites within the channel: calcium binds a more external site, whereas magnesium binds to a location deeper within the pore, consistent with the smaller size of the magnesium ion.

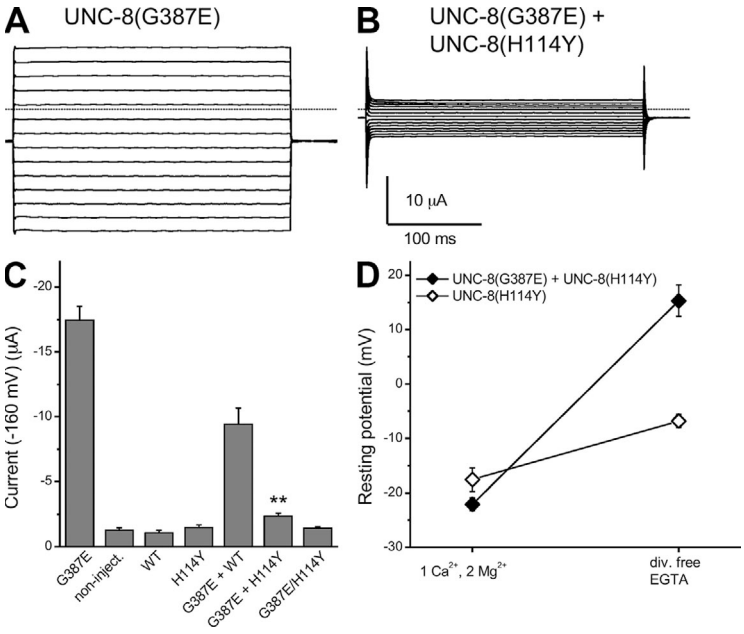


**Figure 7.** UNC-8(H114Y), the trans-suppressor of UNC-(G387E) neuronal swelling, suppresses UNC-8(G387E) currents. (A) Example of currents recorded from an oocyte injected with UNC-8(G387E). (B) Example of currents recorded from an oocyte injected with UNC-8(G387E) plus UNC-8(H11Y). Both oocytes were perfused with the divalent cation–free plus EGTA NaCl solution. Currents were elicited by voltage steps from −160 to +100 mV in 20-mV increments from a holding potential of −30 mV. The dashed line corresponds to the zero current level. (C) Average current amplitudes at −160 mV recorded from oocytes injected with UNC-8(G387E) ($n = 23$), noninjected oocytes ($n = 14$), wild-type UNC-8 ($n = 17$), UNC-8(H114Y) ($n = 23$), UNC-8(G387E) plus UNC-8(wt) ($n = 11$), UNC-8(G387E) plus UNC-8(H114Y) ($n = 23$), and UNC-8(G387E/H114Y) ($n = 13$). **, $P \leq 0.01$ by ANOVA. (D) Mean change in resting potential upon switch from NaCl physiological solution containing 1 mM $CaCl_2$ and 2 mM $MgCl_2$ to the divalent cation–free plus EGTA NaCl solution in oocytes injected with UNC-8(H114Y) (open diamonds; $n = 5$) and in oocytes injected with UNC-8(G387E) plus UNC-8(H114Y) (closed diamonds; $n = 13$).

We next wondered whether UNC-8(G387E) high sensitivity to extracellular divalent cations is a general feature of UNC-8 or if it is related to this specific mutation. To discriminate between these two possibilities, we expressed a second UNC-8 mutant protein, UNC-8 (A586T), in *Xenopus* oocytes (Tavernarakis et al., 1997). The A586T missense mutation is located in the extracellular region (Fig. S2). A586T is encoded by the *e49* allele, which also results in uncoordinated movement (Shreffler et al., 1995). Our measurements showed that UNC-8(A586T) produces outwardly rectifying currents that are 20 times larger in the absence of divalent cations than in physiological NaCl solution (Fig. 6, A–D). These results support the idea that the blockage by extracellular divalent cations is likely an intrinsic feature of UNC-8 channels.

### Effect of trans-suppressor mutation H114Y on UNC-8(G387E) currents

An intragenic suppressor mutation was isolated in a genetic screen for mutations that influence *unc-8(d)*–induced neuronal swelling (Shreffler et al., 1995). H114Y (*e15lb129* allele) suppresses the Unc-8(d) neuronal swelling and uncoordinated phenotypes in either the cis or trans configuration to the G387E mutation. This result is consistent with a model in which the H114Y mutation disrupts either assembly or function of UNC-8 in a multimeric channel. H114 corresponds to a highly conserved residue located in the intracellular N-terminal region adjacent to the first transmembrane domain (Fig. S2, A and C). Based on our results, we reasoned that H114Y may reduce neuronal damage by suppressing UNC-8(G387E) currents. To test this idea, we coexpressed UNC-8(H114Y) with UNC-8(G387E) in *Xenopus* oocytes and analyzed current amplitudes. We found that UNC-8(G387E) plus UNC-8(H114Y) currents were smaller than that of UNC-8(G387E) alone (Fig. 7, A–C). In fact, UNC-8(G387E) currents were suppressed ~85% by coexpression with UNC-8(H114Y). Consistent with a smaller current amplitude, the membrane potential of these oocytes on average depolarized to a lower potential upon switching to a divalent cation–free plus EGTA solution as compared with oocytes injected with UNC-8 (G387E) alone (compare Fig. 7 D with Fig. 3 E). To test the effect of H114Y mutation within the same UNC-8 subunit (in cis), we built the UNC-8(G387E/H114Y) double mutant. We found that these channels were not functional in oocytes (Fig. 7 C). Notably, UNC-8(H114Y) did not produce currents when expressed alone, suggesting that this mutant subunit is not hyperactivated (Fig. 7 C). Interestingly, wild-type UNC-8 also suppressed UNC-8(G387E) currents but by a lower degree, which is consistent with the lower neurotoxicity observed in *unc-8(n491)/+* heterozygotes (Shreffler and Wolinsky, 1997). Current suppression by UNC-8(H114Y) could be the result of effects on channel function or trafficking to the cell surface. In any case, our data are consistent with the idea that the level of neurotoxicity of hyperactivated UNC-8 is defined by the amplitude of UNC-8 mutant ionic current.

### Severity of UNC-8 mutations and pH sensitivity

Allele *n49*, which encodes the A586T mutation, causes a less severe uncoordinated phenotype than the *n491* and *e15* alleles that encode G387E mutation (Shreffler et al., 1995). This difference is caused by a lower number of swollen neurons in *n49* versus *n491* and *e15* mutants (Shreffler et al., 1995). Based on our results, we hypothesized that in vivo cationic currents through UNC-8(A586T) channels should be smaller than currents through UNC-8(G387E). We thus compared current amplitudes in oocytes expressing UNC-8(A586T) and

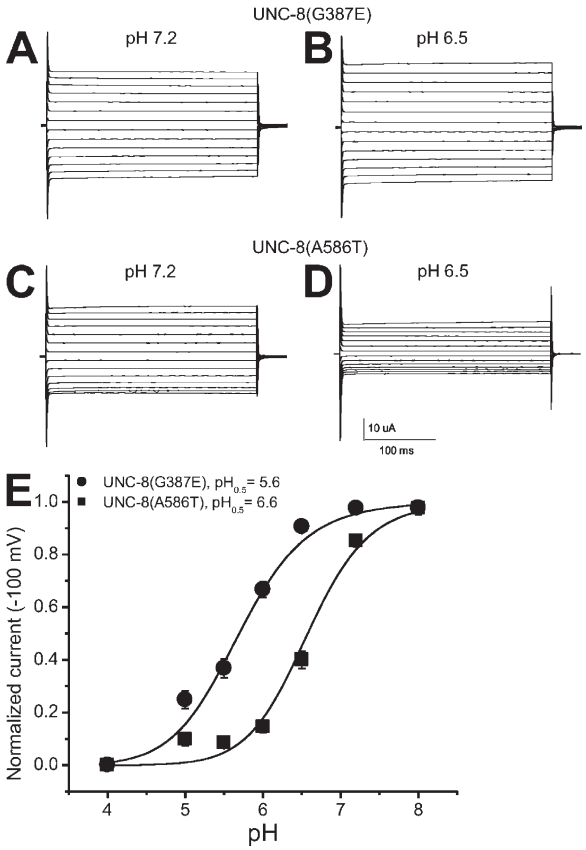


**Figure 8.** pH sensitivity of neurotoxic UNC-8 mutants. (A) Example of currents stimulated by voltage steps from −160 to +100 mV in an oocyte injected with UNC-8(G387E); the holding potential was −30 mV. The oocyte was perfused with the divalent cation–free plus EGTA NaCl solution at pH 7.2. (B) The same oocyte shown in A was perfused with the divalent cation–free plus EGTA NaCl solution at pH 6.5. (C and D) Same as in A and B for an oocyte expressing UNC-8(A586T). (E) pH dose–response curves for oocytes expressing UNC-8(G387E) (closed circles; $n$ = 22) and UNC-8(A586T) (closed squares; $n$ = 14), respectively. Before normalization, all currents were leak subtracted. Data points were fitted by sigmoidal curves that gave $pH_{0.5}$ values of 5.6 and 6.6 for UNC-8(G387E) and UNC-8(A586T), respectively.

UNC-8(G387E), perfused with a divalent cation–free plus EGTA solution. However, we found no statistical difference (10.1 ± 1.8 and 13.3 ± 3.1 μA for A586T and G387E, respectively, at −100 mV, expressed as mean ± SD; $n = 9$ and 15). We next tested whether calcium sensitivity was different in the two mutants. Indeed, because calcium inhibits UNC-8(d) currents, a different sensitivity to this divalent cation could manifest in different current amplitude in vivo. We found that the Ki for calcium was 1.66 μM at −100 mV, which is lower than the Ki we determined for G387E mutant (6 μM at −100 mV).

We next wondered whether UNC-8(G387E) and UNC-8 (A586T) currents were sensitive to pH and if a difference in pH sensitivity could contribute to the difference in the in vivo phenotypes. We analyzed UNC-8(G387E) and UNC-8(A586T) pH sensitivity in *Xenopus* oocytes perfused with solutions with a pH ranging from 5 to 8. We found that both currents were inhibited by acidic pH. However, although UNC-8(G387E) $pH_{0.5}$ was 5.6, UNC-8(A586T) $pH_{0.5}$ was 6.6 (Fig. 8). These data suggest that a smaller fraction of UNC-8(G387E) channels than UNC-8(A586T) channels is inhibited at physiological pH. This effect could account for the observation that *unc-8(n491)* and *unc-8(e15)* corresponding to the G387E mutation result in more neuronal swelling than the *unc-8(n49)* allele that encodes UNC-8(A586T). To conclude, our results show that UNC-8(d) is inhibited by acidic pH and suggest that differences both in calcium and pH sensitivity between the G387E and A586T mutant proteins could contribute to their different toxicities in vivo.

## DISCUSSION

We undertook this study to better characterize neurotoxic mutants of the *C. elegans* DEG/ENaC channel UNC-8 and to establish whether a correlation exists between their level of toxicity and channel properties. By expression in *Xenopus* oocytes, we show that neurotoxic UNC-8(d) mutations induce channel hyperactivation. The strong block exerted by extracellular divalent cations on UNC-8(d) channels diminishes current amplitude and could therefore account for limiting the cellular toxicity of UNC-8(d) channels. Indeed, reduction of extracellular divalent cations concentration resulted in swelling and death of *Xenopus* oocytes expressing UNC-8(d) channels. Further evidence that the current amplitude through the mutant UNC-8 channels defines their level of toxicity is provided by the our findings that: (a) coexpression with an UNC-8 intragenic mutation that suppresses neuronal swelling reduces current amplitude, and (b) the less toxic mutation, UNC-8(A586T), is associated with higher sensitivity to calcium and acidic pH and is therefore expected to produce smaller currents in vivo. Collectively, our data are consistent with the idea that the neurotoxicity of UNC-8 gain-of-function mutants is caused by hyperactive cation transport and that this effect may be quelled in vivo by extracellular divalent cations and pH.

### Channel neurotoxicity and current amplitude

Hyperactivated DEG/ENaC channels can induce swelling and death of the cells in which they are expressed (Driscoll and Chalfie, 1991; Huang and Chalfie, 1994; Xiong et al., 2004). For example, hyperactivation of mouse ASIC1a by prolonged stroke-induced tissue acidosis contributes to neuronal demise (Xiong et al., 2004). Similarly, a mutation in the pore domain hyperactivates the *C. elegans* MEC-4 channel and results in the swelling and death of the touch neurons in which MEC-4 is expressed (Driscoll and Chalfie, 1991; Goodman et al., 2002). Excess ion influx caused by hyperactivation of DEG/ENaCs is thought to result in an ionic imbalance that is ultimately toxic to the cell. MEC-4(d) and ASIC1a have been shown to be calcium permeable, suggesting that at least some neurotoxic DEG/ENaC channels contribute directly to elevation of intracellular calcium and/or trigger calcium release from the ER (Bianchi et al., 2004; Xiong et al., 2004). Blockage of hyperactivated DEG/ENaC channels by the application of amiloride or PcTx1 toxin, an ASIC1-specific inhibitor, significantly improves neuronal survival, supporting the idea that ion influx through these channels is the trigger for neuronal death (Bianchi et al., 2004; Xiong et al., 2004). However, to what extent the amount of $Na^+$ and/or $Ca^{2+}$ influx is toxic and what intrinsic channel properties define its level of toxicity remained unclear.

We report here the functional characterization of neurotoxic mutations in *C. elegans* DEG/ENaC channel UNC-8. Neurotoxic mutations in UNC-8 are unique in that they cause the death of only a fraction of the neurons in which UNC-8 is expressed (Shreffler et al., 1995) (Fig. 1 E). Indeed, DA/DB motor neurons swell during the L1 larval stage, but most (∼65%) recover and survive into adulthood. This result suggests that the neurotoxicity of the UNC-8 mutants is lower than that of other DEG/ENaC channels including MEC-4(d), DEG-1(d), and ASIC1a (Driscoll and Chalfie, 1991; Huang and Chalfie, 1994; Xiong et al., 2004), and that it may be regulated in a cell-specific manner. We found that UNC-8 subunits form homomeric channels in *Xenopus* oocytes and that neurotoxic mutations G387E and A586T cause channel hyperactivation. However, ionic currents are small because of the block exerted by extracellular divalent cations calcium and magnesium. Indeed, with a Ki for calcium of <10 μM, the UNC-8(d) channels G387E and A586T are blocked at physiological calcium concentrations, at least at negative potentials. Perhaps this effect contributes to the relatively low toxicity of UNC-8(d) channels in vivo. On the other hand, the neuronal swelling of UNC-8(d) mutants also suggests that endogenous factors and/or other subunits may at least partially

relieve the calcium block of UNC-8(d) in vivo. When calcium and magnesium are removed, UNC-8(d)–dependent currents in *Xenopus* oocytes are significantly enhanced, and this effect is correlated with oocyte toxicity. Thus, our data support the idea that the current amplitude through neurotoxic DEG/ENaC channels specifies the level of toxicity.

Interestingly, UNC-8 gain-of-function mutants are calcium impermeable, suggesting that excess $Na^+$ influx is sufficient to induce the toxic insult. Elevated $Na^+$ influx could induce reversal of the $Na^+/Ca^{2+}$ exchanger and/or membrane depolarization, resulting in activation of voltage-gated calcium channels. Both of these events are expected to elevate intracellular $Ca^{2+}$. Importantly, block by extracellular divalent cations was observed in both UNC-8(G387E) and UNC-8(A586T) mutants, suggesting that the high sensitivity to extracellular divalent cations is a property of UNC-8 channels and that it is not introduced by either mutation per se.

### Calcium permeability versus calcium block

Our data show that calcium acts as an open channel blocker but does not permeate through UNC-8 gain-of-function mutant channels. In contrast, calcium acts as a permeant blocker on MEC-4(d) (Bianchi et al., 2004; Brown et al., 2008). Interestingly, although the Ki for calcium block in UNC-8(G387E) is in the micromolar range (6 µM at −100 mV), it is in the millimolar range for the MEC-4(d)–MEC-10(d) channel complex (Brown et al., 2008). Moreover, although calcium binds very close to the external mouth of the pore in UNC-8(G387E), it binds to a site deeper in the pore in the MEC-4(d)–MEC-10(d) channel complex (Brown et al., 2008). Other members of the DEG/ENaC family were shown either to be blocked by calcium or to be calcium permeable. For example, calcium-impermeable ASIC3 is blocked by calcium in the nanomolar range, and low pH releases the calcium block (Immke and McCleskey, 2003). Conversely, calcium-permeable ASIC1a is blocked by extracellular calcium with a Ki of ∼5 mM (Paukert et al., 2004). Based on these observations, we speculate that DEG/ENaC channels that have a strong affinity for calcium may not be calcium permeable and vice versa. This prediction is consistent with the fact that tightly bound ions are unlikely to leave a high affinity site to permeate through the channel pore.

Importantly, our data show that despite a strong affinity for calcium and magnesium, caused by the voltage dependence of the block, currents through gain-of-function UNC-8 mutants are still substantial at depolarized potentials. Based on the fact that two different UNC-8 gain-of-function mutations show strong affinity for extracellular divalent cations, we suggest that divalent cation sensitivity is likely a property intrinsic of the UNC-8 channel. Thus, we speculate that wild-type UNC-8 is similarly blocked by extracellular divalent cations. If this is the case, currents through UNC-8 may be regulated by voltage in an indirect way. For example, membrane depolarization associated with neuronal and/or synaptic activity would release calcium and magnesium block, allowing flow of ions through UNC-8. This mechanism could contribute to the recently discovered role for UNC-8 in an activity-dependent mechanism of synaptic remodeling (Petersen et al., 2011; Thompson-Peer et al., 2012; unpublished data).

### Neurotoxic UNC-8 mutations and DEG/ENaC channels structure–function relationships

The two gain-of function UNC-8 mutations that hyperactivate channel function and induce neuronal swelling reside in the UNC-8 extracellular domain. G387E is located in a poorly conserved loop in the "finger" domain, and A586T is positioned in a loop between α 4 and α 5 of the "thumb" domain (Jasti et al., 2007; Gessmann et al., 2010; Eastwood and Goodman, 2012) (Fig. S2 C). Previous studies have shown that the thumb domain participates significantly in proton binding (Immke and McCleskey, 2003; Paukert et al., 2004; Jasti et al., 2007; Wang and Bianchi, 2009; Yang et al., 2009), and that it undergoes substantial movement during gating (Passero et al., 2009). In ASICs, the movement of the thumb domain is translated into channel gating by the π–π interaction between a conserved extracellular tyrosine adjacent to TM1 (Y72 in ASIC1a) and a tryptophan located in a loop between β sheets 9 and 10 (W288 in ASIC1a) (Li et al., 2009). These gating residues are conserved in UNC-8 (Fig. S2 A). Our data are consistent with the idea that in UNC-8 channels, mutations that may perturb the movement of the thumb domain shift the channel into a hyperactivated mode, thereby stabilizing the channel open state, as suggested by previous studies (Hong et al., 2000; Yang et al., 2009). Thus, our data and previous published work support the idea that the thumb domain plays an important role in DEG/ENaC channel gating by diverse stimuli including mechanical forces. Intriguingly, several *mec-4* mutations that result in touch insensitivity cluster around this extracellular region (Tavernarakis et al., 1997; García-Añoveros et al., 1998; Hong et al., 2000).

To conclude, we have characterized the functional properties of the neurotoxic UNC-8 DEG/ENaC protein. Our findings are consistent with the proposal that strong blockage exerted by extracellular divalent cations inhibits UNC-8 channel activity in vivo and that this effect limits the toxicity of UNC-8(d) channels in vivo. We suggest that the extent of divalent cation blockage, in addition to calcium permeability, is a DEG/ENaC channel property that sets the level of toxicity in vivo.

We thank Gerhard Dahl and Charles W. Luetje for providing *Xenopus* oocytes and Jeff Grant for critical reading of the manuscript. Some of the strains used in this work were provided by the *C. elegans* Genetics Center, which is supported by the US

National Institutes of Health (NIH) National Center for Research Resources.

This work was supported by American Cancer Society RGS-09-043-01-DDC and NIH RO1NS070969 grants (to L. Bianchi), NIH RO1NS26115 and R21MH077302 grants (to D.M. Miller), and by Vanderbilt Silvio O. Conte Center grant MH078028 (to T. Miller).

Lawrence G. Palmer served as editor.

Submitted: 11 February 2013
Accepted: 1 July 2013

## REFERENCES

Askwith, C.C., J.A. Wemmie, M.P. Price, T. Rokhlina, and M.J. Welsh. 2004. Acid-sensing ion channel 2 (ASIC2) modulates ASIC1 $H^+$-activated currents in hippocampal neurons. *J. Biol. Chem.* 279:18296–18305. http://dx.doi.org/10.1074/jbc.M312145200

Bianchi, L., and M. Driscoll. 2002. Protons at the gate: DEG/ENaC ion channels help us feel and remember. *Neuron.* 34:337–340. http://dx.doi.org/10.1016/S0896-6273(02)00687-6

Bianchi, L., B. Gerstbrein, C. Frøkjaer-Jensen, D.C. Royal, G. Mukherjee, M.A. Royal, J. Xue, W.R. Schafer, and M. Driscoll. 2004. The neurotoxic MEC-4(d) DEG/ENaC sodium channel conducts calcium: implications for necrosis initiation. *Nat. Neurosci.* 7:1337–1344. http://dx.doi.org/10.1038/nn1347

Brenner, S. 1974. The genetics of *Caenorhabditis elegans*. *Genetics.* 77:71–94.

Brown, A.L., S.M. Fernandez-Illescas, Z. Liao, and M.B. Goodman. 2007. Gain-of-function mutations in the MEC-4 DEG/ENaC sensory mechanotransduction channel alter gating and drug blockade. *J. Gen. Physiol.* 129:161–173. http://dx.doi.org/10.1085/jgp.200609672

Brown, A.L., Z. Liao, and M.B. Goodman. 2008. MEC-2 and MEC-6 in the *Caenorhabditis elegans* sensory mechanotransduction complex: Auxiliary subunits that enable channel activity. *J. Gen. Physiol.* 131:605–616. http://dx.doi.org/10.1085/jgp.200709910

Calavia, M.G., J.A. Montaño, O. García-Suárez, J. Feito, M.A. Guervós, A. Germanà, M. Del Valle, P. Pérez-Piñera, J. Cobo, and J.A. Vega. 2010. Differential localization of acid-sensing ion channels 1 and 2 in human cutaneus pacinian corpuscles. *Cell. Mol. Neurobiol.* 30:841–848. http://dx.doi.org/10.1007/s10571-010-9511-2

Canessa, C.M., J.D. Horisberger, and B.C. Rossier. 1993. Epithelial sodium channel related to proteins involved in neurodegeneration. *Nature.* 361:467–470. http://dx.doi.org/10.1038/361467a0

Chalfie, M., and E. Wolinsky. 1990. The identification and suppression of inherited neurodegeneration in *Caenorhabditis elegans*. *Nature.* 345:410–416. http://dx.doi.org/10.1038/345410a0

Chandrashekar, J., C. Kuhn, Y. Oka, D.A. Yarmolinsky, E. Hummler, N.J. Ryba, and C.S. Zuker. 2010. The cells and peripheral representation of sodium taste in mice. *Nature.* 464:297–301. http://dx.doi.org/10.1038/nature08783

Chelur, D.S., G.G. Ernstrom, M.B. Goodman, C.A. Yao, L. Chen, R. O'Hagan, and M. Chalfie. 2002. The mechanosensory protein MEC-6 is a subunit of the *C. elegans* touch-cell degenerin channel. *Nature.* 420:669–673. http://dx.doi.org/10.1038/nature01205

Driscoll, M., and M. Chalfie. 1991. The mec-4 gene is a member of a family of *Caenorhabditis elegans* genes that can mutate to induce neuronal degeneration. *Nature.* 349:588–593. http://dx.doi.org/10.1038/349588a0

Eastwood, A.L., and M.B. Goodman. 2012. Insight into DEG/ENaC channel gating from genetics and structure. *Physiology (Bethesda).* 27:282–290. http://dx.doi.org/10.1152/physiol.00006.2012

García-Añoveros, J., C. Ma, and M. Chalfie. 1995. Regulation of *Caenorhabditis elegans* degenerin proteins by a putative extracellular domain. *Curr. Biol.* 5:441–448. http://dx.doi.org/10.1016/S0960-9822(95)00085-6

García-Añoveros, J., J.A. García, J.D. Liu, and D.P. Corey. 1998. The nematode degenerin UNC-105 forms ion channels that are activated by degeneration- or hypercontraction-causing mutations. *Neuron.* 20:1231–1241. http://dx.doi.org/10.1016/S0896-6273(00)80503-6

Gessmann, R., N. Kourtis, K. Petratos, and N. Tavernarakis. 2010. Molecular modeling of mechanosensory ion channel structural and functional features. *PLoS ONE.* 5:e12814. http://dx.doi.org/10.1371/journal.pone.0012814

Goodman, M.B., G.G. Ernstrom, D.S. Chelur, R. O'Hagan, C.A. Yao, and M. Chalfie. 2002. MEC-2 regulates *C. elegans* DEG/ENaC channels needed for mechanosensation. *Nature.* 415:1039–1042. http://dx.doi.org/10.1038/4151039a

Graham, R.W., K. Van Doren, S. Bektesh, and E.P. Candido. 1988. Maturation of the major ubiquitin gene transcript in *Caenorhabditis elegans* involves the acquisition of a trans-spliced leader. *J. Biol. Chem.* 263:10415–10419.

Han, L., Y. Wang, R. Sangaletti, G. D'Urso, Y. Lu, S. Shaham, and L. Bianchi. 2013. Two novel DEG/ENaC channel subunits expressed in glia are needed for nose-touch sensitivity in *Caenorhabditis elegans*. *J. Neurosci.* 33:936–949. http://dx.doi.org/10.1523/JNEUROSCI.2749-12.2013

Hitomi, Y., A. Suzuki, Y. Kawano, K. Nozawa-Inoue, M. Inoue, and T. Maeda. 2009. Immunohistochemical detection of ENaCbeta in the terminal Schwann cells associated with the periodontal Ruffini endings of the rat incisor. *Biomed. Res.* 30:113–119. http://dx.doi.org/10.2220/biomedres.30.113

Hong, K., I. Mano, and M. Driscoll. 2000. In vivo structure-function analyses of *Caenorhabditis elegans* MEC-4, a candidate mechanosensory ion channel subunit. *J. Neurosci.* 20:2575–2588.

Huang, M., and M. Chalfie. 1994. Gene interactions affecting mechanosensory transduction in *Caenorhabditis elegans*. *Nature.* 367:467–470. http://dx.doi.org/10.1038/367467a0

Hummler, E., P. Barker, J. Gatzy, F. Beermann, C. Verdumo, A. Schmidt, R. Boucher, and B.C. Rossier. 1996. Early death due to defective neonatal lung liquid clearance in alpha-ENaC-deficient mice. *Nat. Genet.* 12:325–328. http://dx.doi.org/10.1038/ng0396-325

Immke, D.C., and E.W. McCleskey. 2003. Protons open acid-sensing ion channels by catalyzing relief of $Ca^{2+}$ blockade. *Neuron.* 37:75–84. http://dx.doi.org/10.1016/S0896-6273(02)01130-3

Jasti, J., H. Furukawa, E.B. Gonzales, and E. Gouaux. 2007. Structure of acid-sensing ion channel 1 at 1.9 Å resolution and low pH. *Nature.* 449:316–323. http://dx.doi.org/10.1038/nature06163

Kocsis, E., B.L. Trus, C.J. Steer, M.E. Bisher, and A.C. Steven. 1991. Image averaging of flexible fibrous macromolecules: the clathrin triskelion has an elastic proximal segment. *J. Struct. Biol.* 107:6–14. http://dx.doi.org/10.1016/1047-8477(91)90025-R

Li, T., Y. Yang, and C.M. Canessa. 2009. Interaction of the aromatics Tyr-72/Trp-288 in the interface of the extracellular and transmembrane domains is essential for proton gating of acid-sensing ion channels. *J. Biol. Chem.* 284:4689–4694. http://dx.doi.org/10.1074/jbc.M805302200

Lingueglia, E., J.R. de Weille, F. Bassilana, C. Heurteaux, H. Sakai, R. Waldmann, and M. Lazdunski. 1997. A modulatory subunit of acid sensing ion channels in brain and dorsal root ganglion cells. *J. Biol. Chem.* 272:29778–29783. http://dx.doi.org/10.1074/jbc.272.47.29778

Park, E.C., and H.R. Horvitz. 1986. Mutations with dominant effects on the behavior and morphology of the nematode *Caenorhabditis elegans*. *Genetics.* 113:821–852.

Passero, C.J., S. Okumura, and M.D. Carattino. 2009. Conformational changes associated with proton-dependent gating of ASIC1a.

*J. Biol. Chem.* 284:36473–36481. http://dx.doi.org/10.1074/jbc.M109.055418

Paukert, M., E. Babini, M. Pusch, and S. Gründer. 2004. Identification of the $Ca^{2+}$ blocking site of acid-sensing ion channel (ASIC) 1: Implications for channel gating. *J. Gen. Physiol.* 124:383–394. http://dx.doi.org/10.1085/jgp.200308973

Petersen, S.C., J.D. Watson, J.E. Richmond, M. Sarov, W.W. Walthall, and D.M. Miller III. 2011. A transcriptional program promotes remodeling of GABAergic synapses in *Caenorhabditis elegans*. *J. Neurosci.* 31:15362–15375. http://dx.doi.org/10.1523/JNEUROSCI.3181-11.2011

Price, M.P., G.R. Lewin, S.L. McIlwrath, C. Cheng, J. Xie, P.A. Heppenstall, C.L. Stucky, A.G. Mannsfeldt, T.J. Brennan, H.A. Drummond, et al. 2000. The mammalian sodium channel BNC1 is required for normal touch sensation. *Nature.* 407:1007–1011. http://dx.doi.org/10.1038/35039512

Price, M.P., S.L. McIlwrath, J. Xie, C. Cheng, J. Qiao, D.E. Tarr, K.A. Sluka, T.J. Brennan, G.R. Lewin, and M.J. Welsh. 2001. The DRASIC cation channel contributes to the detection of cutaneous touch and acid stimuli in mice. *Neuron.* 32:1071–1083. http://dx.doi.org/10.1016/S0896-6273(01)00547-5

Schoenmakers, T.J., G.J. Visser, G. Flik, and A.P. Theuvenet. 1992. CHELATOR: an improved method for computing metal ion concentrations in physiological solutions. *Biotechniques.* 12:870–874.

Sherwood, T., R. Franke, S. Conneely, J. Joyner, P. Arumugan, and C. Askwith. 2009. Identification of protein domains that control proton and calcium sensitivity of ASIC1a. *J. Biol. Chem.* 284:27899–27907. http://dx.doi.org/10.1074/jbc.M109.029009

Shi, S., D.D. Ghosh, S. Okumura, M.D. Carattino, O.B. Kashlan, S. Sheng, and T.R. Kleyman. 2011. Base of the thumb domain modulates epithelial sodium channel gating. *J. Biol. Chem.* 286:14753–14761. http://dx.doi.org/10.1074/jbc.M110.191734

Shreffler, W., and E. Wolinsky. 1997. Genes controlling ion permeability in both motorneurons and muscle. *Behav. Genet.* 27:211–221. http://dx.doi.org/10.1023/A:1025605929373

Shreffler, W., T. Magardino, K. Shekdar, and E. Wolinsky. 1995. The unc-8 and sup-40 genes regulate ion channel function in *Caenorhabditis elegans* motorneurons. *Genetics.* 139:1261–1272.

Sluka, K.A., M.P. Price, N.M. Breese, C.L. Stucky, J.A. Wemmie, and M.J. Welsh. 2003. Chronic hyperalgesia induced by repeated acid injections in muscle is abolished by the loss of ASIC3, but not ASIC1. *Pain.* 106:229–239. http://dx.doi.org/10.1016/S0304-3959(03)00269-0

Smith, C.J., J.D. Watson, M.K. VanHoven, D.A. Colón-Ramos, and D.M. Miller III. 2012. Netrin (UNC-6) mediates dendritic self-avoidance. *Nat. Neurosci.* 15:731–737. http://dx.doi.org/10.1038/nn.3065

Syntichaki, P., K. Xu, M. Driscoll, and N. Tavernarakis. 2002. Specific aspartyl and calpain proteases are required for neurodegeneration in *C. elegans*. *Nature.* 419:939–944. http://dx.doi.org/10.1038/nature01108

Tavernarakis, N., W. Shreffler, S. Wang, and M. Driscoll. 1997. unc-8, a DEG/ENaC family member, encodes a subunit of a candidate mechanically gated channel that modulates *C. elegans* locomotion. *Neuron.* 18:107–119. http://dx.doi.org/10.1016/S0896-6273(01)80050-7

Thompson-Peer, K.L., J. Bai, Z. Hu, and J.M. Kaplan. 2012. HBL-1 patterns synaptic remodeling in *C. elegans*. *Neuron.* 73:453–465. http://dx.doi.org/10.1016/j.neuron.2011.11.025

Wang, Y., and L. Bianchi. 2009. Insights into the molecular determinants of proton inhibition in an acid-inactivated degenerins and mammalian epithelial $Na^+$ channel. *Biochemistry.* 48:10005–10013. http://dx.doi.org/10.1021/bi9014902

Wang, Y., A. Apicella Jr., S.K. Lee, M. Ezcurra, R.D. Slone, M. Goldmit, W.R. Schafer, S. Shaham, M. Driscoll, and L. Bianchi. 2008. A glial DEG/ENaC channel functions with neuronal channel DEG-1 to mediate specific sensory functions in *C. elegans*. *EMBO J.* 27:2388–2399. http://dx.doi.org/10.1038/emboj.2008.161

Wemmie, J.A., C.C. Askwith, E. Lamani, M.D. Cassell, J.H. Freeman Jr., and M.J. Welsh. 2003. Acid-sensing ion channel 1 is localized in brain regions with high synaptic density and contributes to fear conditioning. *J. Neurosci.* 23:5496–5502.

White, J.G., E. Southgate, J.N. Thomson, and S. Brenner. 1986. The structure of the nervous system of the nematode *Caenorhabditis elegans*. *Philos. Trans. R. Soc. Lond. B Biol. Sci.* 314:1–340. http://dx.doi.org/10.1098/rstb.1986.0056

Woodhull, A.M. 1973. Ionic blockage of sodium channels in nerve. *J. Gen. Physiol.* 61:687–708. http://dx.doi.org/10.1085/jgp.61.6.687

Xiong, Z.G., X.M. Zhu, X.P. Chu, M. Minami, J. Hey, W.L. Wei, J.F. MacDonald, J.A. Wemmie, M.P. Price, M.J. Welsh, and R.P. Simon. 2004. Neuroprotection in ischemia: blocking calcium-permeable acid-sensing ion channels. *Cell.* 118:687–698. http://dx.doi.org/10.1016/j.cell.2004.08.026

Xu, K., N. Tavernarakis, and M. Driscoll. 2001. Necrotic cell death in *C. elegans* requires the function of calreticulin and regulators of $Ca^{2+}$ release from the endoplasmic reticulum. *Neuron.* 31:957–971. http://dx.doi.org/10.1016/S0896-6273(01)00432-9

Yang, H., Y. Yu, W.G. Li, F. Yu, H. Cao, T.L. Xu, and H. Jiang. 2009. Inherent dynamics of the acid-sensing ion channel 1 correlates with the gating mechanism. *PLoS Biol.* 7:e1000151. http://dx.doi.org/10.1371/journal.pbio.1000151

Zhang, P., and C.M. Canessa. 2002. Single channel properties of rat acid–sensitive ion channel-1α, -2a, and -3 expressed in *Xenopus* oocytes. *J. Gen. Physiol.* 120:553–566. http://dx.doi.org/10.1085/jgp.20028574

Zhang, W., L. Bianchi, W.H. Lee, Y. Wang, S. Israel, and M. Driscoll. 2008. Intersubunit interactions between mutant DEG/ENaCs induce synthetic neurotoxicity. *Cell Death Differ.* 15:1794–1803. http://dx.doi.org/10.1038/cdd.2008.114